RSC Advances

ROYAL SOCIETY OF CHEMISTRY

www.rsc.org/advances

Efficient photocatalysts from polymorphic cuprous oxide/zinc oxide microstructures

Ru Li[†], Liangmin Yu[†], Xuefeng Yan[†*], Qunwei Tang[‡*]

[†] Key Laboratory of Marine Chemistry Theory and Technology, Ministry of Education, Ocean University of China, Qingdao 266100, P.R. China;

[‡] Institute of Materials Science and Engineering, Ocean University of China, Qingdao 266100, P.R. China.

*E−mail address: yanxuefeng@ouc.edu.cn; tangqunwei@ouc.edu.cn

Abstract: Pursuit of robust and cost−effective photocatalysts has been a persistent objective for environmental pollution problems. Polymorphic Cu_2O/ZnO microstructures are successfully fabricated by a mild solution strategy. The integration of Cu_2O with ZnO is a facile approach of creating and separating photoelectrons and holes, leading to the high photodegradation efficiency against methyl orange dye under simulated light irradiation. Detailed investigations are carried out by adjusting Cu^{2+}/Zn^{2+} ratio to optimize the resultant morphology and therefore photocatalytic activity. 87.6% of methyl orange dyes have been photodegradated over 5.5 h−light irradiation. Notably, a pseudo cell comprising a Cu_2O/ZnO photoanode, a Pt counter electrode, and a methyl orange aqueous solution is pioneerly designed to demonstrate the potential mechanism for photoelectrochemical reaction.

1 Introduction

Cuprous oxide (Cu_2O) is a *p*−type semiconductor metal oxide with a direct band gap of about

1.9~2.2 eV. The easy fabrication and cost−effectiveness of Cu_2O, as well as its high abundance, environmental friendliness and unique optical, electrical, and magnetic properties [1−3] have demonstrated Cu_2O to be promising in solar energy conversion,[4,5] catalysis, [6−10]electrode materials,[11] sensors,[12−14] and magnetic storage devices.[15] The shape−controlled synthesis of Cu_2O micro/nano−crystals has achieved much success in recent years. Yu *et al* prepared Cu_2O nanowires and sheets by a liquid phase reduction process with polyacrylamide as the template.[16] Other structures such as cubes,[17−19] octahedral,[6] polyhedral with high-index planes,[20,21] spheres,[12,22,23] and nanocages can also be fabricated by reducing $Cu(OH)_2$ or $Cu(OH)_4^{2-}$ species. Although many achievements have been made by creating novel morphologies and developing new applications, a remaining problem for Cu_2O is the easy recombination of photogenerated electrons and holes, leading to a modest photocatalytic activity. By addressing this issue, well−designed structures from noble metals such as Au, Ag, Pt, Pd, etc. have been widely employed to decorate metal oxides to elevate the electron−hole separation.[24−26] Considering the high expense and limited mineral sources of noble metals, researchers have distracted their attention to the coupling of two semiconductors possessing different redox energy levels for their corresponding conduction and valence bands, which has been proved to be an attractive approach to achieve more efficient charge separation, to increase the lifetime of the charge carriers, and to enhance the efficiency of the interfacial charge transfer to adsorbed dyes.[27−29]

In order to search for other robust and cost−effective photocatalysts, we present here a new class of Cu_2O/ZnO crystals by a simple mild solution strategy, in which copper sulfate, zinc chloride, sodium hydroxide, and glucose monohydrate are involved as starting materials with no assistance of organic compounds or surfactants. The photocatalytic performances derived from the resultant Cu_2O/ZnO crystals are evaluated by decomposing methyl orange (MO) dye. More importantly, a

potential mechanism for enhancing photocatalytic activity is proposed on the basis of a pseudo cell. The photoelectrochemical results reveal the remarkably enhanced photocatalysis benefiting from facile photogenerated electron–hole separation. It is expected that the current work may provide a new paradigm for the construction of narrow band–gap semiconductor polymorphic microstructures as promising and versatile photocatalysts.

2 Experimental

2.1 Materials and reagents

All the chemical reagents such as copper sulfate ($CuSO_4 \cdot 5H_2O$, 99.0%, Tianjin Regent Chemicals Co., Ltd), zinc chloride ($ZnCl_2$, 98.0%, Sinopharm Chemical Reagent Co., Ltd), sodium hydroxide (NaOH, 96.0%, Tianjin Reagent No.3 Plant), glucose monohydrate ($C_6H_{12}O_6 \cdot H_2O$, Sinopharm Chemical Reagent Co., Ltd) were of analytical grade and used without further purification. Commercial MO was used as a target dye. All the aqueous solutions were prepared with deionized water (DI Water).

2.2 Synthesis of Cu_2O/ZnO crystals

The synthesis procedures of Cu_2O were as follows: 800 mL of NaOH (1.0 M) aqueous solution and 40 mL of $C_6H_{12}O_6 \cdot H_2O$ (1.0 M) solution were added into 200 mL of 20 wt% $CuSO_4$ aqueous solution and $ZnCl_2$ aqueous solution with varied stoichiometries at 25 °C under vigorous agitation. The reactant was heated at 70 °C for 15 min and then cooled to room temperature. The resultant crystals were thoroughly rinsed through DI water and ethanol, and finally vacuum dried at 60 °C. As a comparison, pristine ZnO was also synthesized at the same conditions whit no $CuSO_4$ in the process. A schematic diagram of the preparation procedure is given in Fig. 1 and the morphologies along with synthesis conditions of the Cu_2O are summarized in Table 1.

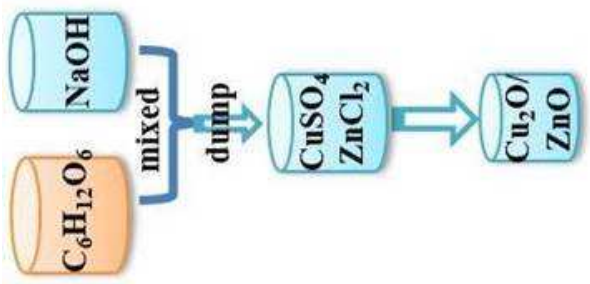

Fig. 1 Schematic diagram for the synthesis Cu_2O/ZnO microcrystals.

Table 1 Summary of reaction conditions and morphology of the resultant Cu_2O/ZnO crystals.

Samples	Cu/Zn molar ratio	Morphology	Degradation rate (%)
Cu_2O	—	Octahedron	37.3
ZnO	—	Amorphous granular	38.0
A_1	1:0.025	Octahedron	—
A_2	1:0.05	Octahedron	—
A_3	1:0.08	Octahedron/flowers	61.3
A_4	1:0.1	Octahedron/flowers	77.8
A_5	1:0.15	Octahedron/flowers	87.6
A_6	1:0.2	Octahedron/flowers	70.0
A_7	1:0.25	Octahedron/flowers	—
A_8	1:0.3	Octahedron/polyhedron	—
A_9	1:0.5	Polyhedron	38.3
A_{10}	1:0.8	Sphere	—
A_{11}	1:1	Sphere	31.6

2.3 Photocatalytic experiments

The photocatalytic activities of the photocatalysts toward MO aqueous solution were performed at ambient atmosphere and room temperature. The procedures were described in details: 0.06 g of the prepared samples was dispersed into 500 mL of MO aqueous solution (0.2 g L^{-1}). The suspensions were vigorously agitated in the dark for 60 min to reach adsorption equilibrium of MO molecules on Cu_2O/ZnO microcrystals. The photocatalytic reaction was conducted in a 500 mL−cylindrical glass vessel fixed in the SGY−IB photochemical reactor (Nanjing Stonetech Electric Equipment Co., Ltd) with a Hg lamp (500 W) as a light source. At regular intervals, a 10 mL of the suspension was sampled and separated by centrifugation at 6000 rpm for 12 min (Hitachi CF15RXII). The residual dye concentration in the supernatant was measured by UV−vis spectrometer (Hitachi UV−3010) at

maximum absorption wavelength of 464 nm for MO aqueous solution. Parallel degradation reactions under the same condition were conducted at intervals.

2.4 Design and photoelectrochemical characterizations of pseudo cells

The strategy of designing pseudo cells was confirmed by following experimental procedures: 1.25 g of poly(vinylidene fluoride) (PVDF) powders were dissolved into *N*–methylpyrrolidone to form a 100 mL of homogeneous solution. The PVDF implanted Cu_2O/ZnO colloids were prepared by mixing PVDF solution and Cu_2O/ZnO microcrystals at a mass ratio of 1: 20. The PVDF implanted Cu_2O/ZnO films on FTO glass substrates (sheet resistance 12 Ω sq^{-1}, purchased from Hartford Glass Co., USA) were prepared coating the PVDF implanted Cu_2O/ZnO colloids onto the glass substrates. The thickness and active area were controlled at ~0.4 μm and ~0.4 cm^2, respectively. Finally, the FTO glass supported Cu_2O/ZnO films were vacuumly dried at 50 °C for 10 h. The Pt CE (300~400 μm in thickness) was purchased from Dalian HepatChroma SolarTech Co., Ltd. The pseudo cells were sealed by a hot–melt Surlyn film (30 μm in thickness) and subsequently hot–pressing. The MO solution was injected into the pseudo cell from the hole on the back of the Pt CE.

The electrochemical performances were recorded on a conventional CHI660E setup (Shanghai Chenhua Device Company, China) comprising an Ag/AgCl reference electrode, a counter electrode (CE) of platinum sheet, and a working electrode of FTO glass supported PVDF implanted Cu_2O/ZnO micro/nanostructure. Electrochemical impedance spectroscopy (EIS) measurements were carried out in a frequency range of 0.01 Hz ~ 10^6 kHz and at an ac amplitude of 10 mV. The photoelectrochemical tests of the Cu_2O/ZnO were carried out by measuring the current–voltage (*J*–*V*) characteristic curves under irradiation of a simulated solar light from a 100 W xenon arc lamp (XQ–500 W) in ambient atmosphere. The incident light intensity was calibrated using a FZ–A type radiometer from Beijing Normal University Photoelectric Instrument Factory to control it at 100

mW cm^{-2} (AM 1.5). Each photovoltaic test was repeated at least 3 times and a compromise $J-V$ curve was employed.

2.5 Other characterizations

The morphologies of the Cu_2O/ZnO photocatalysts were observed on a scanning electron microscope (SEM S4800). The XRD profiles were collected in a scan mode at a scan speed of 4 ° min^{-1} in the 2θ range between 20 and 80°. Transmission electron microscope (TEM) and high−resolution transmission electron microscopy (HRTEM) images were obtained by a JEOL model JEM2010, JEOL2010 instrument at an accelerating voltage of 200 kV. UV−vis diffuse reflectance spectroscopy (DRS) was performed on a Hatachi UV−4100 spectrometer.

3 Results and discussion

3.1 Morphological observation and formation mechanism

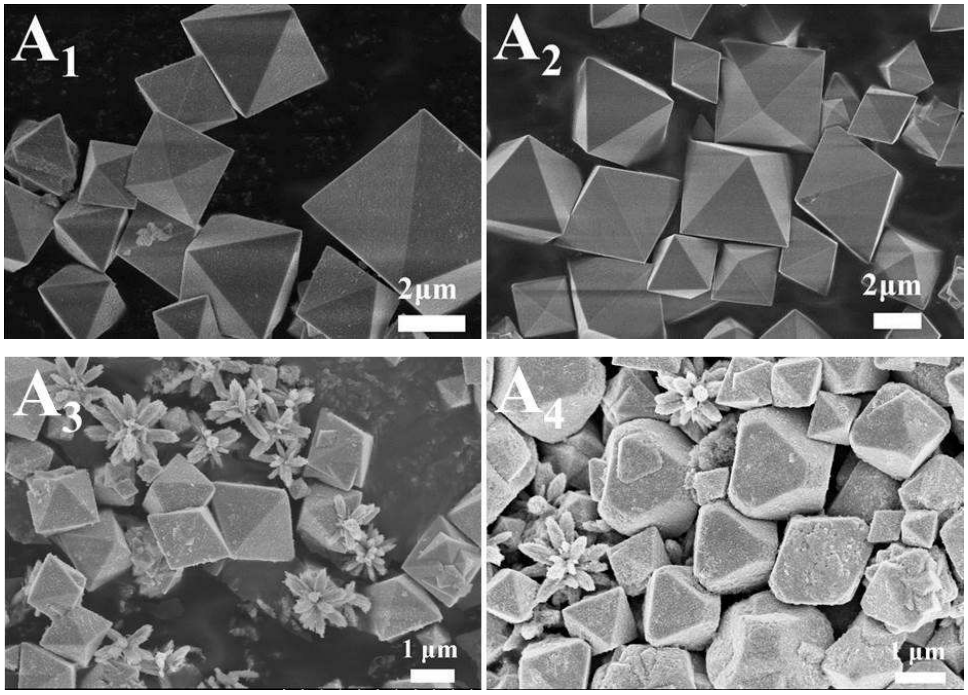

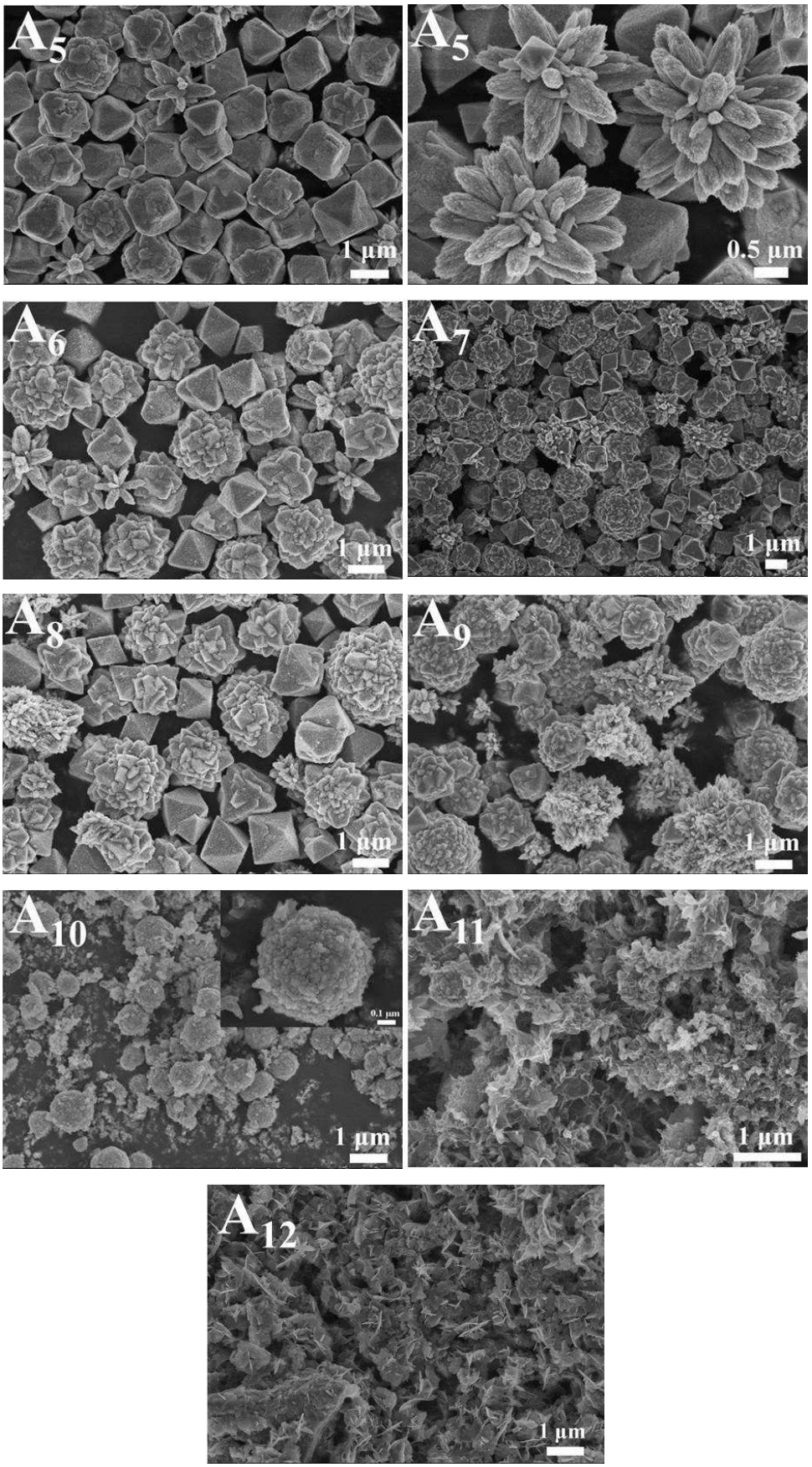

Fig. 2 SEM images of the Cu_2O/ZnO photocatalysts synthesized at various $[Cu^{2+}]/[Zn^{2+}]$ ratio. From

images A_1 to A_{11}: 1:0.025, 1:0.05, 1:0.08, 1:0.1, 1:0.15, 1:0.2, 1:0.25, 1:0.3, 1:0.5, 1:0.8, and 1:1.0. Image A12 presents the SEM morphology of pristine ZnO.

The representative SEM photographs in Fig. 2 show that the morphologies of Cu_2O/ZnO microstructures synthesized at molar ratios of $[Cu^{2+}]/[Zn^{2+}]$: 1:0.025, 1:0.05, 1:0.08, 1:0.1, 1:0.15, 1:0.2, 1:0.25, 1:0.3, 1:0.5, 1:0.8, and 1:1.0 and pristine ZnO, respectively. Well−defined octahedron structures can be obtained at $[Cu^{2+}]/[Zn^{2+}]$ ratio of 1:0.025 and 1:0.05, as shown in Fig. $2A_1$ and A_2. With further elevation in $[Zn^{2+}]$ dosage, octahedron grew radially from the same center to yield a flower−like morphology with an average diameter of 1.5 μm and octahedron particle size of 1.5 μm (Fig. $2A_3$−A_7) at $[Cu^{2+}]/[Zn^{2+}]$ of 1:0.08, 1:0.1, 1:0.15, 1:0.2 and 1:0.25, giving a homogeneous particle size.[30] At a $[Cu^{2+}]/[Zn^{2+}]$ ratio of 1:0.3 and 1:0.5, the as−prepared Cu_2O/ZnO microcrystals in Fig. $2A_8$ and A_9 are polyhedron with particle size of around 1.5 μm. Further increase in $[Cu^{2+}]/[Zn^{2+}]$ from 1:0.8 to 1:1.0 (Fig. $2A_{10}$ and A_{11}) results in decreased size and increased roughness, the shape of the Cu_2O/ZnO microcrystal become a microsphere. Notably, the morphologies of Cu_2O/ZnO at high $[Zn^{2+}]$ dosage such as at a $[Cu^{2+}]/[Zn^{2+}]$ ratio of 1:1.0 tend to be similar to that of neat ZnO, as shown in Fig. $2A_{12}$. From the morphological evolution patterns, one can see that an increase in $[Cu^{2+}]/[Zn^{2+}]$ molar ratio leads to morphological conversion from regular octahedron to flower−like and finally to microsphere. We can facilely control the specific surface area of the resultant Cu_2O/ZnO by adjusting $[Cu^{2+}]/[Zn^{2+}]$ molar ratio.

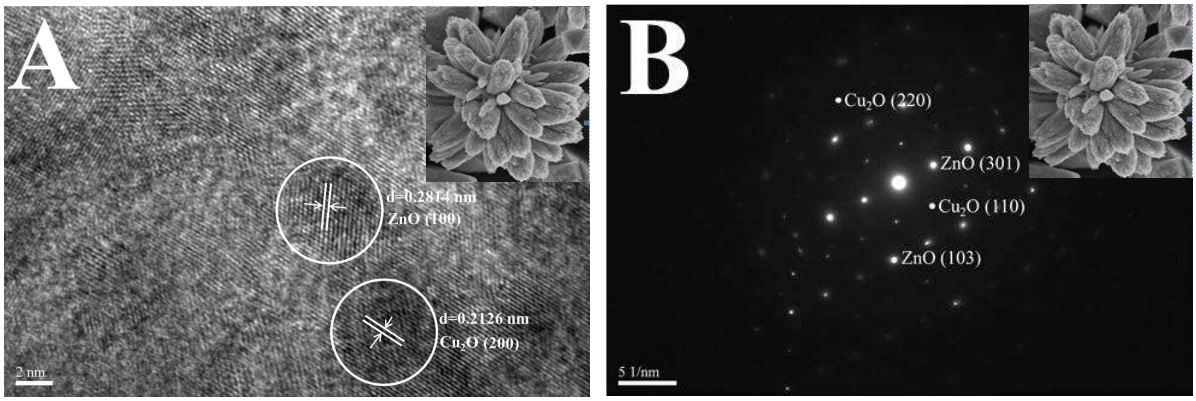

Fig. 3 Morphological characterizations of the Cu_2O/ZnO−1:0.15 microstructure: (A) HRTEM photograph, (B) SAED pattern.

Fig. 3A shows the high resolution transmission electron microscopy (HRTEM) photograph of the Cu_2O/ZnO photocatalyst synthesized at a $[Cu^{2+}]/[Zn^{2+}]$ ratio of 1:0.15. It is noticeable that the clear lattice fringes of 0.2814 and 0.2126 nm correspond to the (100) and (200) planes of ZnO and Cu_2O, respectively. The clear crystals suggest that Cu_2O/ZnO has good crystallinity, whereas the enormous crystal defects provide more active sites for dye adsorption and photodegradation. Selected area electron diffraction (SAED) pattern (Fig. 3B) corresponding to the polymorphic Cu_2O/ZnO−1:0.15 reveals a characteristic of single crystals.

3.2 Structure analysis

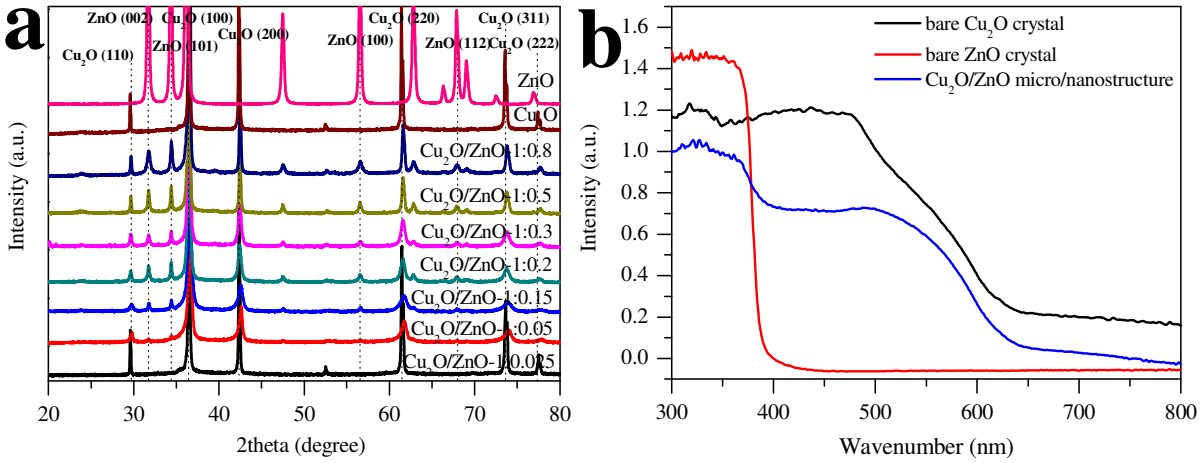

Fig. 4 (a) XRD patterns of the pristine ZnO, Cu_2O and various Cu_2O/ZnO photocatalysts. (b) UV−vis diffuse reflectance spectra (DRS) of pristine Cu_2O, ZnO particles, and Cu_2O/ZnO−1:0.15.

Fig. 4a displays XRD patterns of the resultant Cu_2O/ZnO photocatalysts. As a reference, the diffraction pattern for pristine Cu_2O is also provided. Apparently, the peaks ascribed to cubic cuprite typed Cu_2O (JCPDS no. 05−0667) and hexagonal wurtzite typed ZnO (JCPDS no. 89−1397) can be detected in the Cu_2O/ZnO photocatalysts. The results from XRD analysis is in an agreement with HRTEM and SAED characterization. The crystallite size can be determined from the broadening of

corresponding XRD peaks by Scherrer formula.[31] No Cu and CuO phases are detected in the Cu_2O/ZnO microcrystals.

$$L = \frac{K\lambda}{\beta \cos\theta} \quad (1)$$

where L is the crystallite size, λ is the wavelength of the X−ray radiation (CuK_α = 0.15418 nm), K is usually taken as 0.89, and β is the full width at half−maximum height (FWHM). In addition, the crystal lattice distortion ($\Delta d/d$) can also be evaluated from the equation,[32] and the structural parameters are summarized in Table 2.

$$\frac{\Delta d}{d} = \frac{\beta}{4tg\theta} \quad (2)$$

At the first glance, all the diffraction peaks are ascribed to the diffraction faces of Cu_2O and ZnO. The crystallite size has a peak valley at Cu_2O/ZnO−1:0.15, whereas the calculated $\Delta d/d$ value is the highest, demonstrating that Cu_2O/ZnO−1:0.15 can provide more active sites for MO adsorption and photodegradation.

Table 2 Structural parameters extracted from XRD patterns.

Microcrystals	β	2θ (°)	Crystallite size (nm)	$\Delta d/d$	τ (ms)
Cu_2O	0.0034	36.56	42.5038	0.0026	0.217
Cu_2O/ZnO−1:0.025	0.0025	36.47	57.7907	0.0019	—
Cu_2O/ZnO−1:0.05	0.0025	36.45	58.8725	0.0019	—
Cu_2O/ZnO−1:0.08	0.0061	36.67	23.6982	0.0046	—
Cu_2O/ZnO−1:0.1	0.0073	36.69	19.8037	0.0055	0.733
Cu_2O/ZnO−1:0.15	0.0101	36.65	14.3119	0.0076	1.186
Cu_2O/ZnO−1:0.2	0.0088	36.56	16.4219	0.0066	0.942
Cu_2O/ZnO−1:0.25	0.0059	36.54	24.4923	0.0045	0.466
Cu_2O/ZnO−1:0.3	0.0054	36.54	26.7601	0.0041	0.438
Cu_2O/ZnO−1:0.5	0.0037	36.56	39.0576	0.0028	—
Cu_2O/ZnO−1:0.8	0.0032	36.49	45.1512	0.0024	—

In order to describe photo−absorption behaviors of the Cu_2O/ZnO photocatalysts, the UV−vis DRS were recorded and shown in Fig. 4b. As comparisons, the absorption spectra of pristine Cu_2O and ZnO are also conducted at the same conditions. The absorption peak at around 340 nm for

commercialized ZnO nanoparticles is assigned to ground excitonic state of ZnO. The UV−Vis absorption spectrum of Cu_2O is characterized by a broad absorption peak from 400 to 600 nm. The appearance of a fluctuation at wavelength lower than 590 nm further indicates that the resultant copper oxide is Cu_2O instead of CuO. Reflectance spectra have been converted to the absorbance spectra using Kubelka−Munk equations (Eqs 3&4).[33−36]

$$F(R_\infty(\lambda)) = \frac{(1-R_\infty)^2}{2R_\infty} \quad (3)$$

$$R_\infty = \frac{R}{R_{BaSO4}} \quad (4)$$

where R is the reflectance recorded for a sample and R_{BaSO4} is the reflectance recorder for a reference. To calculate the band−gap energy, the Kubelka−Munk function is converted to the form $(F(R\infty)E)^{1/2}$ and the wavelength is changed to energy units (eV). The band gap energy can be recorded by an extrapolation method (see Fig. 5). The band gaps (E_g) of pristine Cu_2O, ZnO, and Cu_2O/ZnO synthesized at $[Cu^{2+}]/[Zn^{2+}]$ ratio of 1:0.08, 1:0.1, 1:0.15, 1:0.2, 1:0.4, 1:0.8 and 1:1 are estimated to be 2.07, 3.30, 2.26, 2.28, 2.30, 2.34, 2.48, 2.61, and 3.12 eV, respectively. Till now, we can make a conclusion that the combination of integration of Cu_2O with ZnO can effectively increase the E_g of pristine Cu_2O, which is superiority to enhance electron−hole pair separation and therefore photocatalytic activity of Cu_2O/ZnO photocatalysts.

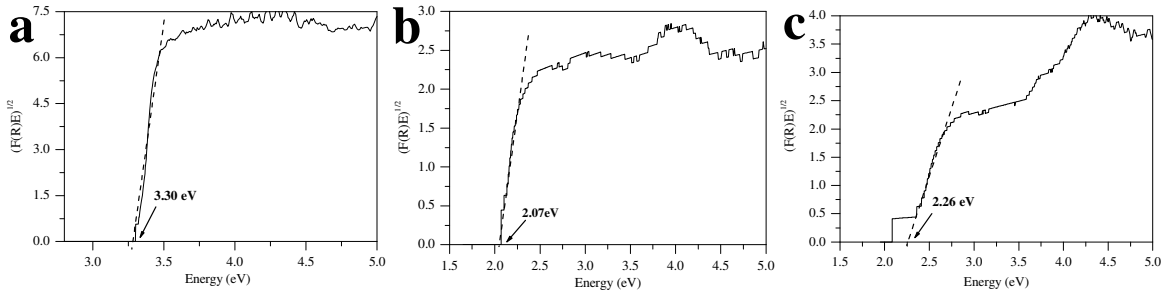

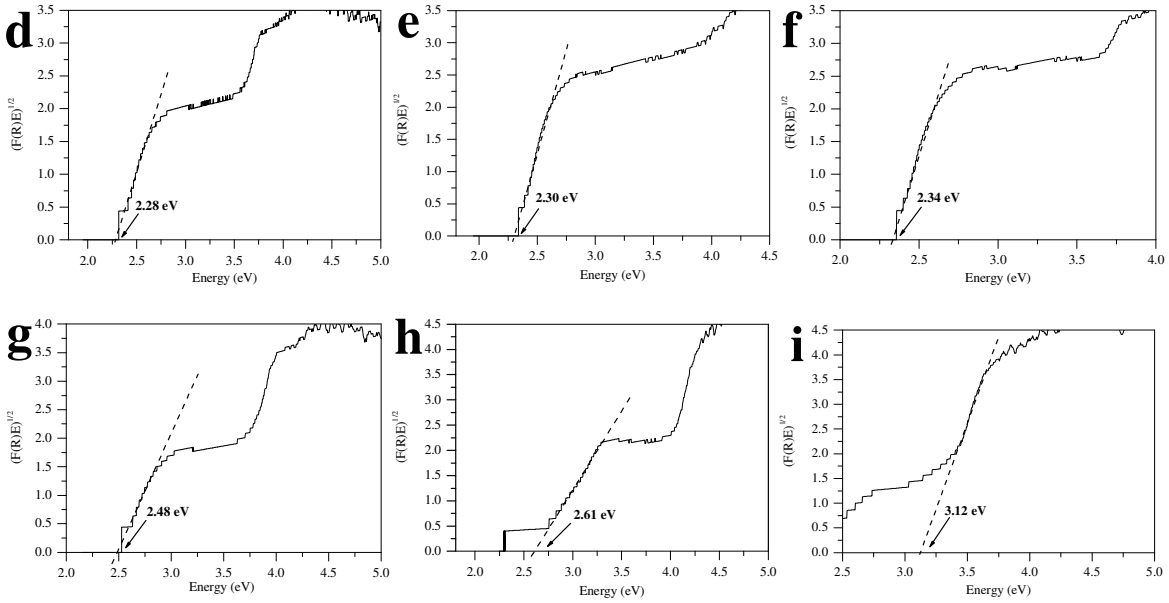

Fig. 5 Determination of the band gap energy values for (a) pure ZnO, (b) pure Cu_2O, and Cu_2O/ZnO synthesized at different mole ratios of $[Cu^{2+}]/[Zn^{2+}]$: (c) 1:0.08, (d) 1:0.1, (e) 1:0.15, (f) 1:0.2, (g) 1:0.4, (h) 1:0.8, (i) 1:1.

3.3 Photocatalytic activity

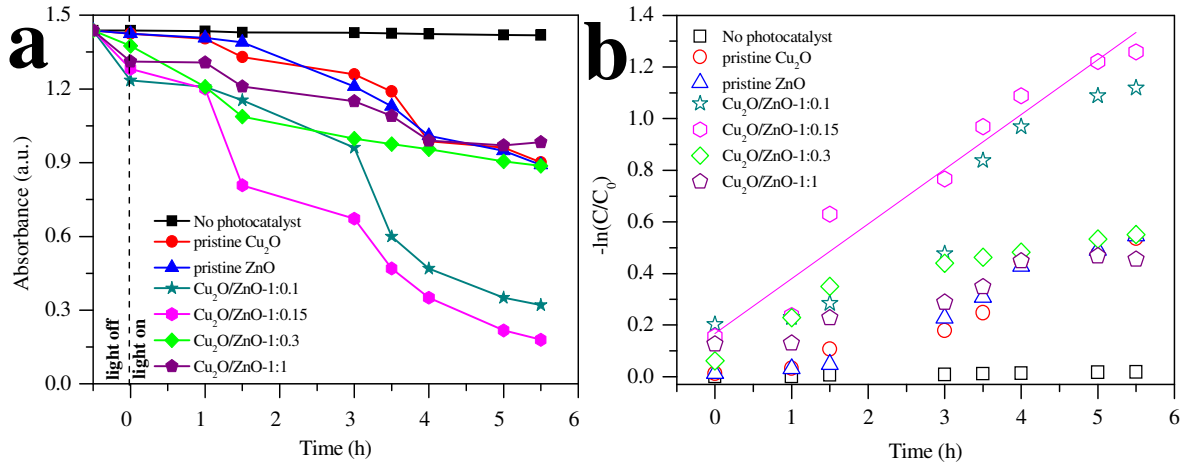

Fig. 6 Time course of the decrease in the (a) absorbance and (b) $-\ln(C/C_0)$ for the photodegradation of MO.

The dependence of absorbance reduction of target dye on photodegradation time is critical to evaluate the photocatalytic activities of photocatalysts.[37,38] Fig. 6 compares the absorbance variations of MO in the presence of Cu_2O/ZnO photocatalysts under light irradiation. Apparently, the

photodegradation kinetics is enhanced by integrating ZnO with Cu_2O in comparison with pristine Cu_2O or ZnO.[39] Direct decomposition of MO without Cu_2O cannot almost be detected under light irradiation in our control experiment (Fig. 6a). It has been reported that Cu_2O and ZnO are typical photocatalysts,[6,39] however, their photocatalytic activities are modest due to easy recombination of photogenerated electrons and holes.[29,40] The Cu_2O/ZnO photocatalyst synthesized at a $[Cu^{2+}]/[Zn^{2+}]$ raito of 1:0.15 exhibits the highest photocatalytic activity, yielding a degradation rate of 87.6% for MO dye over 5.5 h−irradiation. The reaction kinetic of the MO degradation follows a pseudo−first order reaction kinetic model, as shown in Fig. 6b.[41] Good linear correlation (R^2 = 0.955) is observed, suggesting that pseudo−first order reaction model is applicable to the current research. The slope of the fitting line reveal a first−order rate constant, k = 0.212 h^{-1}. Viewed from this point, the elevated specific surface area and exposed facets with high surface energy have acceleration effect to its photocatalytic activity, which is also a golden rule in designing an efficient photocatalyst.

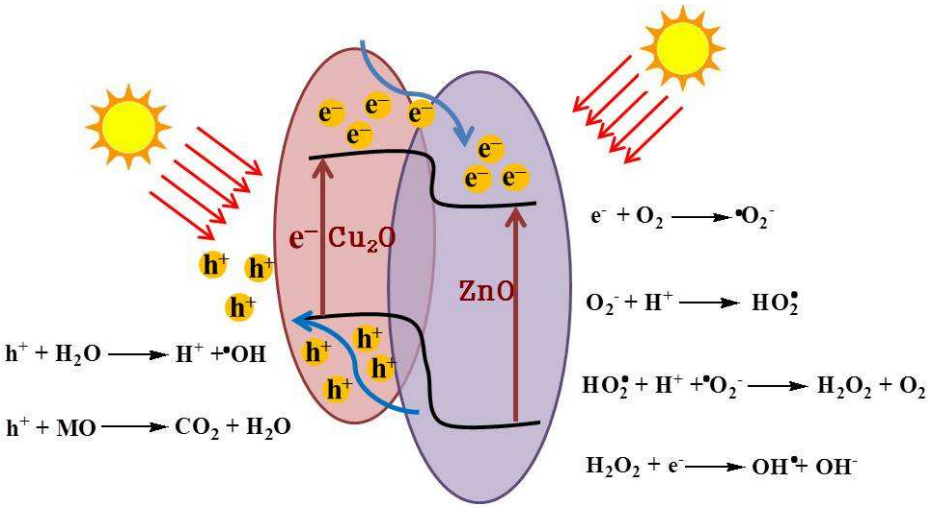

Fig. 7 Schematic diagram for the potential photocatalytic mechanism by Cu_2O/ZnO photocatalyst.

To well understand the potential mechanism for the enhancement in photocatalytic activity, we propose a schematic diagram for electron−hole pair generation and separation, as shown in Fig. 7. Under irradiation by simulated sunlight, the electrons on valence band (VB) of Cu_2O absorb photons

and jump to its conduction band (CB), and subsequently flow to CB of ZnO, leaving holes transfer to an opposite direction. In this fashion, the combination of Cu_2O and ZnO has superiority of separating electron–hole pairs for $OH^{\cdot}$ radical generation.[42] These $OH^{\cdot}$ radicals are crucial oxidative species to react with organic molecules.

3.4 Photoelectrical performances

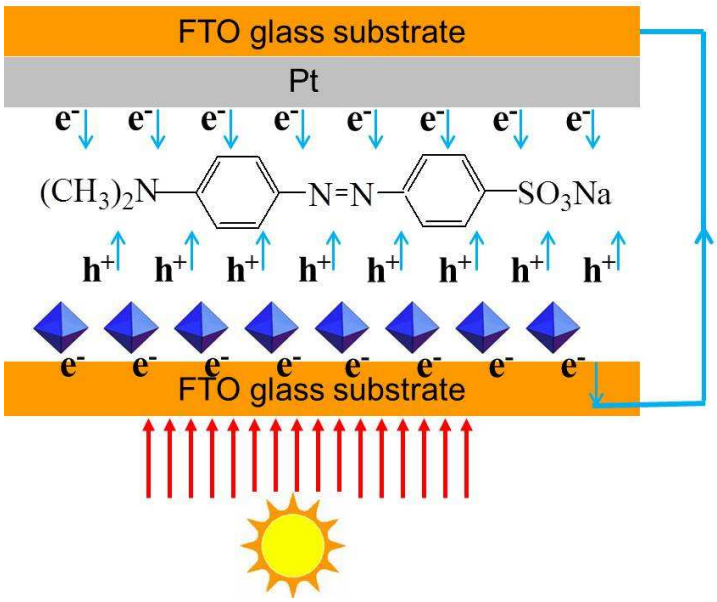

Fig. 8 Schematic of a pseudo cell for MO degradation by Cu_2O/ZnO photocatalyst.

The original intention of combining ZnO with Cu_2O is to enhance the photogenerated electron–hole separation. To realize this objective and reveal the potential mechanism, we present here the successful fabrication of a pseudo cell by sandwiching MO aqueous solution between a photoanode from an FTO glass supported Cu_2O/ZnO anode and an FTO glass supported Pt counter electrode, as shown in Fig. 8. This design is inspirited by the sandwich structure of dye–sensitized solar cells. Under irradiation from anode side, the photogenerated electrons migrate to FTO layer along the conducting channels formed by Cu_2O microcrystallites and then transfer to the Pt counter electrode along external circuit, and photogenerated holes may react with MO molecules, leading to efficient separation of electron–hole pairs. In this fashion, the recorded photocurrent density can be utilized to

compare the photocatalytic reaction kinetic of the Cu_2O/ZnO photocatalyst. This measurement can be performed on a traditional electrochemical workstation. A lower photocurrent density means a lower electron–hole separation, which can also be confirmed by the transient photocurrent responses.

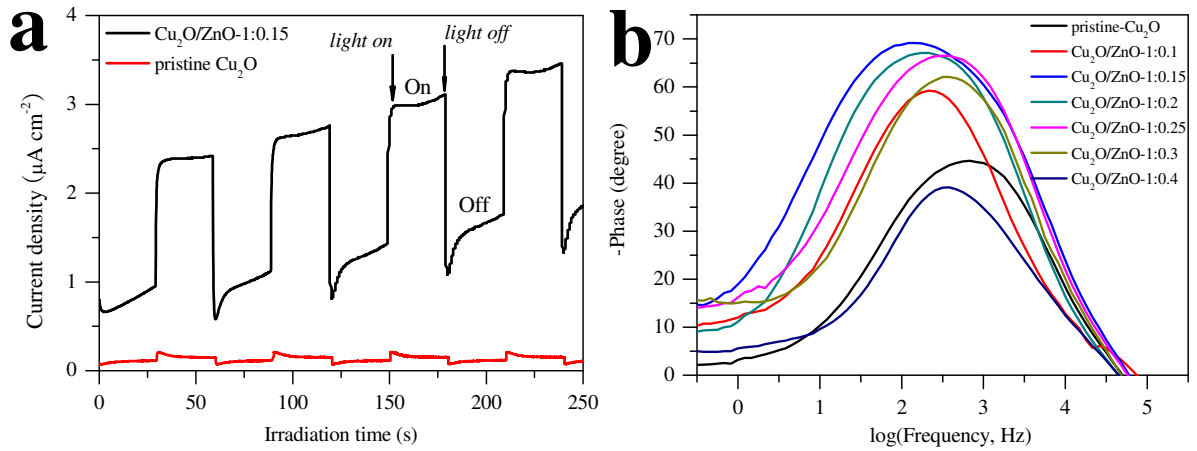

Fig. 9 The (a) transient photocurrent responses and (b) Bode EIS plots of pseudo cells with Cu_2O/ZnO photoanodes.

Fast start-up and multiple start capabilities are two crucial requirements for an efficient photocatalyst. As shown in Fig. 9a, the cell device employing Cu_2O/ZnO anode synthesized at a Cu_2O/ZnO–1:0.15 has a maximum photocurrent density, demonstrating that the Cu_2O/ZnO–1:0.15 photocatalyst is vigorous in generating electron–hole pairs and transferring electrons. An abrupt increase in current density refers to a high kinetics at electron–hole pair generation and separation. Moreover, star/stop cycling can be employed to evaluate the multiple start–up capability of a photocatalyst. After multiple start–up, the cell displays an enhanced photocurrent density, which demonstrates the photocatalytic activity of Cu_2O/ZnO–1:0.15 photocatalyst can be further elevated by elongating irradiation time. In order to better reveal the separation of electron–hole pairs, we recorded the lifetime ($\tau = 1/2\pi f_p$, where f_p is the peak frequency at high frequency) of electrons on photoanode.[43] In the pseudo cell, the photogenerated electrons separate from holes and migrate to

FTO layer, leaving holes transfer to an opposite direction, therefore the τ value is negatively corrected to electron–hole recombination. From Fig. 9b, the τ values are calculated to be 0.733, 1.186, 0.942, 0.466, 0.438, 0.433, and 0.217 ms for Cu_2O/ZnO photocatalysts synthesized at $[Cu^{2+}]/[Zn^{2+}]$ ratios of 1:0.1, 1:0.15, 1:0.2, 1:0.25, 1:0.3, 1:0.4, and pristine Cu_2O, respectively. The results demonstrate that the integration of ZnO can markedly enhance the electron–hole separation of Cu_2O and Cu_2O/ZnO–1:0.15 is the best–defined photocatalyst for MO photodegradation. Although the current research is far from the optimization, the interesting concept in designing efficient photocatalysts along with impressive photocatalytic activities make the polymorphic Cu_2O/ZnO microstructures to be promising candidates for photocatalyst applications.

4 Conclusions

In summary, Cu_2O/ZnO microstructures with controllable morphologies have been successfully synthesized by a mild solution strategy for photocatalyst applications. Experiment results demonstrate that the 87.6% of MO dyes can be photodegradated over 5.5 h–light irradiation in comparison with 37.3% for pristine Cu_2O and 38.0% for ZnO. With an aim of revealing the potential mechanism for enhanced photocatalysis, a pseudo cell is designed by sandwiching methyl orange solution between a Cu_2O/ZnO anode and Pt counter electrode. Due to the rapid electron–hole separation, fast start–up, and high multiple start capability demonstrate the polymorphic Cu_2O/ZnO microstructures to be promising photocatalysts.

Acknowledgements

The authors gratefully acknowledge financial support by the National Natural Science Foundation of China (51102219, 51342008), Fundamental Research Funds for the Central Universities (201113024,

201313042), National Key Technology Support Program (2012BAB15B02), National Key and National Key Technology Support Program (2010AA09Z203, 2010AA065104), the Fundamental Research Funds for the Central Universities (201313042).

Reference

[1] R. Asahi, T. Morikawa, T. Ohwaki, K. Aoki and Y. Taga, *Science,* 2001, **293**, 269.

[2] L. Zhao, X. F. Chen, X. C. Wang, Y. J. Zhang, W. Wei, Y. H. Sun, M. Antonietti and M. M. Titirici, *Adv. Mater.,* 2010, **22**, 3317.

[3] S. Deng, V. Tjoa, H. M. Fan, H. R. Tan, D. C. Sayle, M. Olivo, S. Mhaisalkar, J. Wei and C. H. Sow, *J. Am. Chem. Soc.*, 2012, **134**, 4905.

[4] Y. –E. Gu, Y. Z. zhang, F. Y. Zhang, J. P. Wei, C. M. Wang, Y. L. Du and W. C. Ye, *Electrochim. Acta*, 2010, **56**, 953.

[5] C. M. McShane and K. S. Choi, *J. Am. Chem. Soc.*, 2009, **131**, 2561.

[6] R. Li, X. Yan, Z. M. Zhang, Q. W. Tang and Y. P. pan, *CrystEngComm* 2013, **15**, 10049.

[7] B. White, M. Yin, A. Hall, D. Le, S. Stolbov, T. Rahman, N. Turro and S. O'Brien, *Nano Lett.,* 2006, **6**, 2095.

[8] L. Li, C. Nan, Q. Peng and Y. Li, *Chem. Eur. J.*, 2012, **18**, 10491.

[9] H. Cao, H. Jiang, G. Yuan, Z. Chen, C. Qi and H. Huang, *Chem. Eur. J.,* 2010, **16**, 10553.

[10] Y. Shang, D. Sun, Y. Shao, D. Zhang, L. Guo and S. Yang, *Chem. Eur. J.,* 2012, **18**, 14261.

[11] A. Goyal, A. L. M. Reddy and P. M. Ajayan, *Small*, 2011, **7**, 1709.

[12] J. Zhang, J. Liu, Q. Peng, X. Wang and Y. Li, *Chem. Mater.*, 2006, **18**, 867.

[13] J. H. Zhong, G. R. Li, Z. L. Wang, Y. N. Ou and Y. X. Tong, *Inorg. Chem.,* 2011, **50**, 757.

[14] H. Zhu, J. Wang and G. Xu, *Cryst. Growth Des.,* 2009, **9**, 633.

[15] D. Fishman, C. Faugeras, M. Potemski, A. Revcolevschi and P. van Loosdrecht, *Phys. Rev. B,* 2009, **80**, 045208.

[16] R. Li, L. M. Yu, L. N. Jia, X. F. Yan and L. Dong, *Chin. J. Inorg. Chem.,* 2013, **29**, 265.

[17] K. X. Yao, X. M. Yin, T. H. Wang and H. C. Zeng, *J. Am. Chem. Soc.*, 2010, **132**, 6131.

[18] L. Gou and C. J. Murphy, *J. Mater. Chem.,* 2004, **14**, 735.

[19] C. -H. Kuo, C. -H. Chen and M. H. Huang, *Adv. Funct. Mater.,* 2007, **17**, 3773.

[20] M. Leng, M. Liu, Y. Zhang, Z. Wang, C. Yu, X. Yang, H. Zhang and C. Wang, *J. Am. Chem. Soc.*, 2010, **132**, 17084.

[21] S. Sun, C. Kong, S. Yang, L. Wang, X. Song, B. Ding and Z. Yang, *CrystEngComm* 2011, **13**, 2217.

[22] H. L. Xu and W. Z. Wang, *Angew. Chem. Int. Ed.*, 2007, **46**, 1489.

[23] Y. Chang, J. J. Teo and H. C. Zeng, *Langmuir,* 2005, **21**, 1074.

[24] Z. Z. Han, L. L. Ren, Z. H. Cui, C. Q. Chen, H. B. Pan and J. Z. Chen, *Appl. Catal., B,* 2012, **126**, 298.

[25] N. Morales−Flores, U. Pal and E. S. Mora, *Appl. Catal., A*, 2011, **394**, 269.

[26] L. Q. Jing, B. Q. Wang, B. F. Xin, S. D. Li, K. Y. Shi, W. M. Cai and H. G. Fu, *J. Solid State Chem.,* 2004, **177**, 4221.

[27] Y. Yang, D. S. Kim, Y. Qin, A. Berger, R. Scholz, H. Kim, M. Knez, U. Gosele, *J. Am. Chem. Soc.*, 2009, **131**, 1390.

[28] Y. K. Hsu, H. H. Lin, M. H. Chen, Y. C. Chen and Y. G. Lin, *Electrochim. Acta,* 2014, **144**, 295.

[29] L. Huang, F. Peng, H. J. Wang, H. Yu and Z. Li, *Catal. Commun.,* 2009, **10**, 1839.

[30] M. Patete, X. H. Peng, C. Koenigsmann, Y. Xu, B. Karn and S. S. Wong, *Green Chem.*, 2011, **13**, 482.

[31] Q. H. Zhang, L. Gao and J. K. Guo, *Appl. Catal., B−Environ.*, 2000, **26**, 207.

[32] L. Q. Jing, X. J. Sun, B. F. Xin, B. Q. Wang, W. M. Cai and H. G. Fu, *J. Solid State Chem.,* 2004, **177**, 3375.

[33] G. Kortum, Reflectance Spectroscopy; Springer−Verlag: Berlin (1969).

[34] P. Kubelka and F. Z. Munk, *Tech. Phys.*, 1931, **12,** 593.

[35] W. G. Zhang and P. S. Halasyamani, *Cryst. Growth Des.*, 2012, **12,** 2127.

[36] D. Wodka, E. Bielanska, R.P. Socha, M. E. Wodka, J. Gurgul, P. Nowak, P. Warszynski and Izumi Kumakiri, *ACS Appl. Mater. Interfaces*, 2010, **2,** 1945.

[37] K. M. Parida and S. Parija, *Solar Energy*, 2006, **80**, 1048.

[38] K. M. Parida, S. S. Dash and D. P. Das, *J. Colloid Interf. Sci.*, 2006, **298**, 787.

[39] C. Xu, L. X. Cao, G. Su, W. Liu, H. Liu, Y. Q. Yu and X. F. Qu, *J. Hazard. Mater.,* 2010, **176**, 807.

[40] R. Ullah and J. Dutta, *J. Hazard. Mater.,* 2008, **156**, 194.

[41] S. L. Suib and S. R. Segal, *Chem. Mater.,* 1997, **9**, 2526.

[42] K. –i. Okamoto, Y. Yamamoto, H. Tanaka, M. Tanaka and A. Itaya, *Bull. Chem. Soc. Jpn.,* 1985, **58**, 2015.

[43] T. Hoshikawa, T. Ikebe, R. Kikuchi and K. Eguchi, *Electrochim. Acta*, 2006, **51**, 5286.

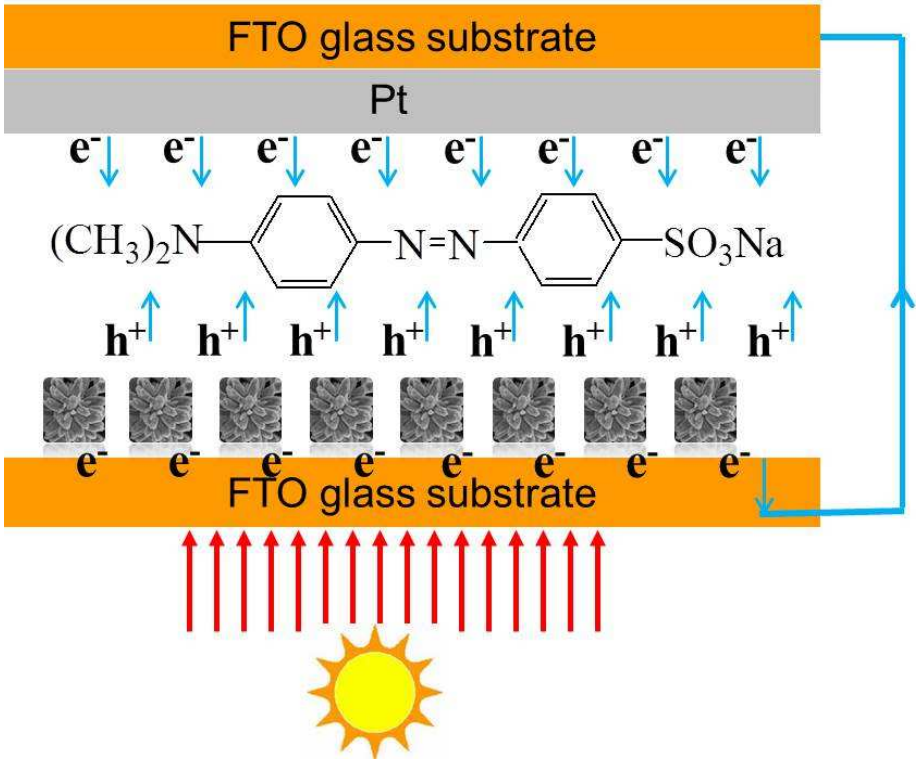

- Polymorphic Cu_2O/ZnO were synthesized by a mild solution method for photocatalysts
- The separation of electron−hole pairs was markedly enhanced
- The resultant Cu_2O/ZnO photocatalysts displayed good photocatalytic activity for methyl orange
- A pseudo photochemical cell was designed to demonstrate the photocatalytic process